

Solar-Powered Environmentally Friendly Hydrogen Production: Advanced Technologies for Sunlight-Electricity-Hydrogen Nexus

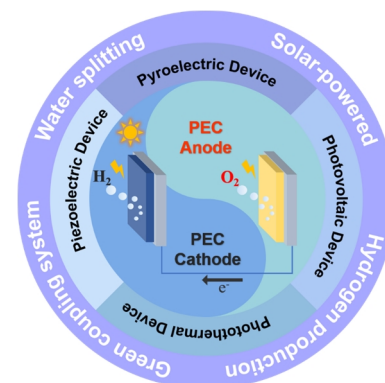
WeiQuan Ji^{1,2#}, Kang Zhang^{1,2#}, Ke Zhan¹, Ping Wang², Xianying Wang^{2*} and Ya Yan^{2*}

¹School of Materials Science and Chemistry, University of Shanghai for Science and Technology, Shanghai 200093, China

²CAS Key Laboratory of Materials for Energy Conversion, Shanghai Institute of Ceramics, Chinese Academy of Sciences (SICCAS), Shanghai 200050, China

ABSTRACT Hydrogen production from water splitting is a clean and sustainable hydrogen production route to alleviate the current energy crisis. However, factors such as energy conversion efficiency, cost-effectiveness, and social benefit limit their industrial application. Therefore, the development of advanced water splitting technologies using clean and renewable energy has become an important research goal of the world. Converting endless solar energy into hydrogen energy directly or indirectly is an effective way to reduce the energy input of hydrogen production. This review focuses on the latest advances in the coupling design of renewable energy supply devices and catalytic electrodes in hydrogen production systems. We not only review the single hydrogen production system based on photochemical, photoelectrochemical, photovoltaic, thermoelectric, pyroelectric, and piezoelectric devices, but also discuss the complex systems of the multiple devices. The structural design of energy supply devices and catalytic electrodes and the study of hydrogen production performance in different systems will be critically discussed in this work. Finally, current challenges and future perspectives of advanced technologies for sunlight-electricity-hydrogen nexus are also presented. It is hoped that this review will provide a timely reference for advancing the development of sunlight-electricity-hydrogen nexus and thus achieve the goal of sustainable production of green hydrogen.

Keywords: water splitting, hydrogen production, green coupling system, sunlight-electricity-hydrogen, structure-activity relations



1 INTRODUCTION

With the rapid development of society, the increasing environmental pollution and energy crisis force the humans to exploit sustainable and green energy sources.^[1-3] Hydrogen, as a renewable clean energy, shows great potential to become the major energy carrier in the future. However, green hydrogen production from renewable energy sources still faces great challenge. According to the International Renewable Energy Agency report, currently about 95% of the hydrogen production originates from fossil fuels.^[4] Therefore, it is necessary to explore efficient energy conversion systems to realize the production of green hydrogen from renewable energy.

As we all know, the energy on earth mainly comes from solar radiation, which is inexhaustible, widely distributed, and available. Therefore, converting solar energy into chemical energy using hydrogen as a carrier is of great strategic significance to solve the energy crisis and realize energy freedom.^[5,6] At present, several hydrogen production systems are designed to use sunlight to produce hydrogen, mainly including photochemical, photoelectrochemical and photovoltaic device hydrogen production systems.^[7,8] To improve the utilization of solar energy, the thermoelectric and pyroelectric devices are also designed to couple with catalytic electrodes. In addition, using vibrational mechanical energy and waste heat to drive water splitting can be used as an auxiliary strategy to facilitate hydrogen production.^[9-11] The solar-to-hydrogen (STH) efficiency is given as an indicator to measure the energy conversion efficiency in different systems.

In this review, the research progress of different hydrogen pro-

duction systems will be firstly introduced, and then the design schemes of energy supply devices and catalytic electrodes in different hydrogen production systems are summarized and discussed, together with the application of multi-system coupling in hydrogen. We hope this review will provide a useful reference for the sustainable production of green hydrogen based on sunlight-electricity-hydrogen nexus.

2 SINGLE HYDROGEN PRODUCTION SYSTEMS

In recent years, the research on water splitting hydrogen production system driven by green renewable energy has attracted widespread attention. Various systems consisting of energy harvesting devices coupled with catalytic electrodes are designed to pursue high hydrogen production efficiency. It mainly includes photochemical, photoelectrochemical hydrogen production systems and photovoltaic, thermoelectric, pyroelectric, and piezoelectric hydrogen production systems. In this part, these renewable energy single hydrogen production systems (SHPS), which serve as a platform to better study the impact of system component design on hydrogen efficiency, will be introduced in detail.

Photochemical Hydrogen Production System. Similar to photosynthesis in plants, photocatalytic hydrogen production is a process that converts solar energy into chemical energy, and it is also considered as a kind of artificial photosynthesis. In this system, when the photocatalyst absorbs photons with energy greater than its band gap ($\geq E_g$), it excites electrons to jump from the valence band to the conduction band, leaving vacancies (known as holes) in the valence band, then the separated electrons and holes are involved in the redox reactions on the photocatalyst surface.^[12-14]

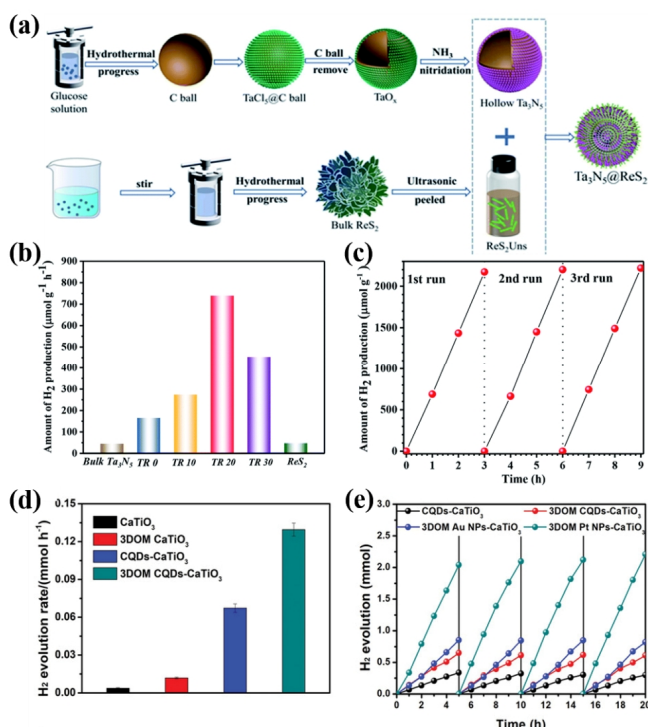


Figure 1. (a) Synthesis schematic of Ta₃N₅@ReS₂.^[15] (b) The photocatalytic H₂-production activities of bulk Ta₃N₅, TR₀, TR₁₀, TR₂₀ and TR₃₀.^[15] (c) Recycling photocatalytic hydrogen evolution test of TR₂₀.^[15] (d) Photocatalytic hydrogen evolution rates of CaTiO₃, 3DOM CaTiO₃, CQDs-CaTiO₃, and 3DOM CQDs-CaTiO₃.^[12] (e) Cycling test of CQDs-CaTiO₃, 3DOM CaTiO₃ with co-catalysts of CQDs, Au NPs, and Pt NPs.^[12]

In recent years, photocatalytic hydrogen evolution has been deeply explored and some progress has been made. However, the solar-to-hydrogen efficiency of photocatalytic hydrogen production is still in the laboratory stage and far from practical application. Nevertheless, many researchers are still devoted to improving the efficiency of photocatalytic water splitting from the following aspects: (I) light absorption; (II) separation and transfer of photogenerated charges; (III) reaction process and mechanism exploration.^[12,15-17]

Low reaction interface, limited active sites, and long carrier transport channels are the main factors limiting the catalytic activity of bulk catalysts. Based on this, Zhan et al. designed a Ta₃N₅ with nano-hollow sphere structure, which can enhance light absorption through multiple reflections, and the inner and outer surfaces can provide more reactive sites compared with bulk Ta₃N₅.^[15] Then, a heterojunction structure was designed by few-layered ReS₂ nanosheets grown on the surface of hollow nanospheres (Figure 1a). This structure can not only increase the response of catalyst in the visible light range, but also increase the edge active sites and promote the separation of photogenerated charges. The obtained Ta₃N₅@ReS₂ showed a high catalytic efficiency for hydrogen evolution reaction (HER) (739.4 μmol g⁻¹ h⁻¹), which is 16.5 and 4.5 times higher than that of bulk and hollow spherical Ta₃N₅, respectively (Figure 1b), and it also exhibits good photocatalytic stability (Figure 1c). In addition to constructing a heterojunction

structure to promote the photocatalytic hydrogen evolution efficiency, the introduction of co-catalysts can promote the separation and transport of photogenerated charges. For example, 3% Pt supported on Ta₃N₅@ReS₂ as a co-catalyst exponentially increased its hydrogen evolution rate (1378.6 μmol g⁻¹ h⁻¹).^[15] However, the scarcity of noble metals seriously hinders their wide application as photocatalytic co-catalysts. As such, Zhao et al. reported the nitrogen and oxygen co-doped carbon quantum dots (CQDs), which was used as a co-catalyst to decorate the three-dimensionally ordered macroporous CaTiO₃ (3DOM CQDs-CaTiO₃).^[18] As can be seen from Figure 1d that the designed 3DOM CQDs-CaTiO₃ achieved a high photocatalytic HER efficiency (0.13 mmol h⁻¹, 20 mg photocatalyst), which exhibits a photocatalytic hydrogen evolution capability close to that of 3DOM Au NPs-CaTiO₃, but it is still not comparable to that of 3DOM Pt NPs-CaTiO₃ (Figure 1e). Therefore, designing efficient co-catalysts that can replace noble metals is also an effective strategy to reduce costs and improve the photocatalytic hydrogen evolution ability.

Photoelectrochemical Hydrogen Production System. Both photocatalytic systems and photoelectrochemical catalytic systems employ photoactive semiconductors as the main active components, but the conditions that lead to excellent performance are different in the two systems. In photocatalytic system, semiconductor catalyst molecules are usually suspended in solution, and redox reactions occur simultaneously on their surfaces. While the redox reactions in the photoelectrochemical system take place on the surface of the photoanode and photocathode, respectively, and the photoactive semiconductor materials are supported on the conductive substrate. From the distribution of light irradiation, the light distribution is unidirectional for the photoelectrochemical system, while three-dimensional for particle suspensions in photocatalytic system. The advantage of photoelectrochemical system compared to the photocatalytic system lies in that the external bias voltage can continuously provide the carrier transport path. The photogenerated charges move to the photoanode and photocathode surfaces respectively under the action of an applied voltage, and then participate in redox reactions.^[19,20] To advance the large-scale application of electrochemical hydrogen production, the most important task is to develop stable, efficient, and cost-effective photocathode and photoanode.

Photocathode. In this system, the photocathode that catalyzes the reduction reaction is usually a p-type semiconductor. Metal oxide is the preferred material for photocathode due to its low-cost, good stability and simple synthesis procedure.^[21,22] However, the poor charge carrier migration of metal oxides seriously hinders its photoelectrochemical hydrogen evolution efficiency. In order to solve this problem, the cocatalyst MoS₂ was used to modify the CuBi₂O₄ photocathode to enhance the PEC performance.^[21] Correspondingly, the prepared CuBi₂O₄@MoS₂ exhibits better catalytic current density (0.182 mA cm⁻²) at 0.6V vs RHE, compared with bare CuBi₂O₄ (0.082 mA cm⁻²), which is attributed to the low interface charge transfer resistance. Therefore, the introduction of cocatalysts to enhance the carrier separation efficiency and interfacial charge transfer of photocatalysts is an effective strategy

to improve their hydrogen production efficiency.

Featured with small band gap and excellent photocorrosion resistance, Sb_2Se_3 semiconductor is also widely used as photocathode to catalyze the HER. By addressing the anisotropic properties of Sb_2Se_3 , Yang et al. synthesized well-defined compact Sb_2Se_3 thin films using a sublimation method in the confined space.^[23] Then, a CdS layer was inserted into Sb_2Se_3 and TiO_2 to increase the initial potential, thereby increasing the half-cell (HC) STH efficiency from 2.33% to 3.4%. The photoelectrochemical cell consisted a Sb_2Se_3 photocathode and a BiVO_4 photoanode, and a STH efficiency of 1.5% was reached with over 10 h stability performance under simulated standard air mass (AM) 1 sun illumination (Figure 2a). Similarly, Li et al. reported a high efficiency Sb_2Se_3 photocathode modified with a $\text{Cd}_x\text{Zn}_{1-x}\text{S}$ buffer and a Pt cocatalyst.^[24] The results showed that Zn/Cd ratio has a consequential influence on the photoelectrochemical performance of $\text{Pt}/\text{Cd}_x\text{Zn}_{1-x}\text{S}/\text{Sb}_2\text{Se}_3$ photocathode and the doping of Zn not only increases the photocurrent density, but also improves the fill factor and efficiency. The optimal photocurrent density of $\text{Pt}/\text{Cd}_x\text{Zn}_{1-x}\text{S}/\text{Sb}_2\text{Se}_3$ photocathode is 17.5 mA cm^{-2} at 0 V vs RHE. Then, $\text{Pt}/\text{Cd}_{0.5}\text{Zn}_{0.5}\text{S}/\text{Sb}_2\text{Se}_3$ and BiVO_4 were used to form an independent coupled solar water splitting system, which achieved a HC-STH efficiency of 2.19% and an impressive stability over 8.5 h without obvious degradation.

Photoanode. Photoanode in the PEC system takes the responsibility of catalyzing the oxygen evolution reaction (OER). The slow reaction kinetics of OER depends heavily on efficient photoanode materials. Since Fujishima and Honda first reported the water splitting in a PEC cell using TiO_2 ,^[25,26] many reports have focused on the research and preparation of photoanode materials for OER.^[27,28] However, the large band gap of 3.0 eV for TiO_2 makes it excited only by ultraviolet light, which accounts for only

4% of sunlight. This greatly limits the effective application of TiO_2 in sustainable photo splitting of water.^[29] Therefore, much more efforts have been devoted to developing efficient catalytic materials to manufacture high-performance, stable and cheap photoelectric electrodes.^[26]

Construction of heterojunctions is one of the most common strategies to improve performance of photoelectrodes. It can enhance the light absorption ability of photoelectrode by adjusting the energy band gap, and also play a role in inhibiting the recombination of photogenerated carriers. For instance, the ferroelectric polarization of BaTiO_3 (BTO) helps to facilitate charge separation and transfer, however, the inherent wide bandgap of BTO limits its utilization in PEC water splitting. In order to overcome this issue, Li et al. reported a simple electrodeposition manner to load Cu_2O nanoparticles on the surface of BTO to fabricate the $\text{BTO}/\text{Cu}_2\text{O}$ heterojunction photoanode (Figure 2b), in which Cu_2O has a small band gap of 2.1 eV with excellent visible light trapping capacity.^[30] Compared with bare BTO, the photocurrent density of all $\text{BTO}/\text{Cu}_2\text{O}$ photoanodes is evidently increased. The maximum STH efficiency of $\text{BTO}/\text{Cu}_2\text{O}$ -100 is 0.11% at 0.72 V vs RHE, which is about twice as much as bare BTO. With a similar strategy, Zhu et al. constructed a $\text{Cu}_2\text{S}/\text{BiVO}_4$ heterostructure photoanode for overall water splitting.^[31] The bare BiVO_4 yielded a photocurrent density of only 2.03 mA cm^{-2} at 1.23 V vs RHE. After modification with Cu_2S and CoFe-OH , the $\text{Cu}_2\text{S}/\text{BiVO}_4$ hybrid photoanode exhibited a photocurrent density of almost 3.07 mA cm^{-2} . Apart from constructing heterojunction, surface modification of the photoanode materials is also a promising direction to meliorate PEC performance.^[32,33] Hematite ($\alpha\text{-Fe}_2\text{O}_3$) is an up-and-coming photoanode material with a conjectural STH efficiency of 15.4%, and its performance can be optimized by decorating cocatalyst on its surface.^[26] Jiao et al. used Zr-based metal-organic frameworks as precursor to construct a thin Fe_2ZrO_5 layer on the surface of

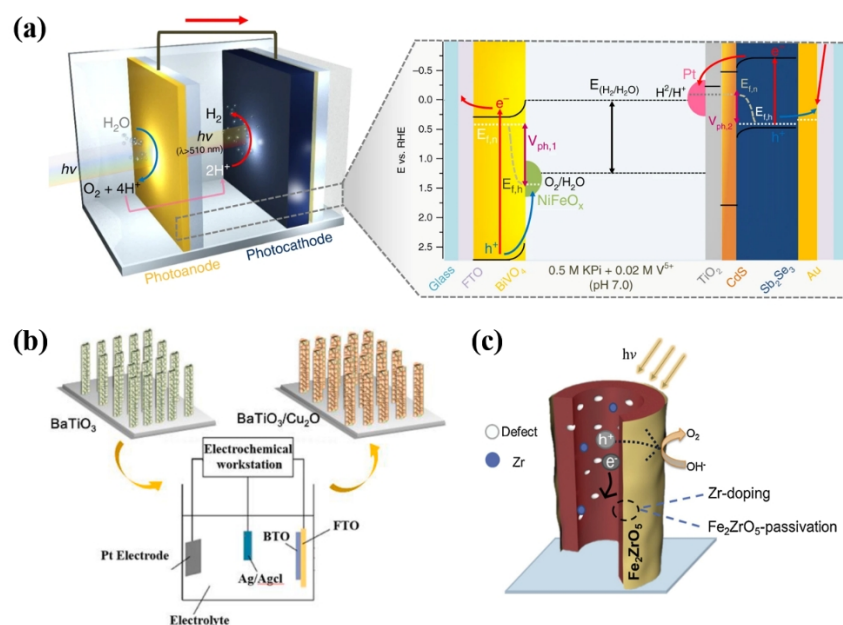


Figure 2. (a) Scheme for the constructed tandem cell.^[23] (b) Illustration for the $\text{BTO}/\text{Cu}_2\text{O}$ heterostructure.^[26] (c) Working mechanism illustration of $\text{Fe}_2\text{ZrO}_5\text{-Fe}_2\text{O}_3$.^[34]

Table 1. Performance of Tandem Cells for PEC Water Splitting

Photoanode	Photocathode	HC-STH (%)	STH (%)	Durability (h)	Ref
NiFeO _x /H, Mo:BiVO ₄	Pt/TiO ₂ /CdS/Sb ₂ Se ₃ /Au	3.4	1.5	10	[21]
CoPi/BiVO ₄	Pt/Cd _{0.5} Zn _{0.5} S/Sb ₂ Se ₃	2.19	0.68	8.5	[24]
Mo:BiVO ₄	Cu/Cu ₂ O/Ga ₂ O ₃ /TiO ₂ /NiMo	-	3	12	[35]
Co ₄ O ₄ /pGO/BiVO ₄ /SnO _x	Pt/TiO _x /PIP/CuO _x	-	4.3	-	[37]
BiVO ₄	Pt-HfO ₂ /CdS/HfO ₂ /CZTS	7.27	3.17	60	[38]
Pt	Pt/TiO ₂ /Sb ₂ Se ₃ /Mo	1.36	-	2	[39]
BiVO ₄	Pt/CdS/ClGS	12.5	3.7	-	[40]
Fe ₂ O ₃	TiO ₂ /Pt/Si	-	0.91	10	[41]
CoFeO _x /BiVO ₄	Pt/TiO ₂ /CdS/CGIZS	-	1.1	1	[42]

Fe₂O₃ (Figure 2c).^[34] The as-prepared Fe₂ZrO₅ as a surface passivation layer can effectively passivate surface defects, which can enhance the separation of photogenerated carriers, inhibit their recombination, and ultimately greatly meliorate the PEC performance of Fe₂O₃. The photocurrent density of Fe₂ZrO₅ modified Fe₂O₃ is 1.65 mA cm⁻² at 1.23 V vs RHE, almost twice higher than that of original hematite. By integrating Ti-based treatment and deposition of Co-Pi co-catalyst, Fe₂ZrO₅-layer decorated Fe₂O₃ photoanode finally displayed a current density of 2.88 mA cm⁻² at the same voltage, almost 3 times higher than the bare Fe₂O₃.

In addition to using a single photoelectrode to achieve PEC-catalyzed water splitting, the PEC system integrating both photoanode and photocathode can not only diminish the applied bias, but also achieve PEC water splitting spontaneously.^[35] Song et al. designed and evaluated a tandem PEC cell with W:BiVO₄ and CuBi₂O₄ as photoanode and photocathode for the overall water splitting, respectively.^[36] However, the unprotected CuBi₂O₄ may undergo photo-corrosion under light in aqueous solution, so it is very unstable. In this work, by using the CdS/TiO₂ heterojunction layer as a protective layer and RuO_x as the co-catalyst, the problem of photo-corrosion was solved. The formed CuBi₂O₄/CdS/TiO₂/RuO_x showed a more negative photocurrent onset potential than the unprotected CuBi₂O₄. Inspired by natural photosynthesis, Ye et al. reported an advanced photoelectrochemical platform with efficient charge-transfer mediators to assist overall water splitting.^[37] The system consists of Co₄O₄/pGO/BiVO₄/SnO_x as photoanode coupled with Pt/TiO_x/PIP/CuO_x as photocathode. They chose partially oxidized graphene (pGO) and SnO_x as mediators for charge transfer. Meanwhile, they constructed an efficient photocathode by using Pt as the HER catalyst and the organic polymer semiconductor PBDB-T:ITIC:PC₇₁BM (PIP) to enhance the light harvesting range (500–800 nm), CuO_x and TiO_x to facilitate the charge transfer ability. The dual-photoelectrode PEC device displayed a potential of about 0.6 V to reach the photocurrent density of 3.5 mA cm⁻², corresponding to a STH efficiency of 4.3%. Therefore, it is believed that while the photocathode material achieves outstanding performance, the photoanode with excellent performance is of great importance. Table 1 is given to visually compare the solar-to-hydrogen efficiencies of different catalytic electrodes.

Photovoltaic Device Hydrogen Production System. Compared with the photochemical and photoelectrochemical hydrogen production systems, using photovoltaic (PV) devices to drive

electrolytic water splitting can achieve higher STH efficiency and excellent hydrogen evolution durability. In this section, some significant examples of coupling solar cells to electrolyzers will be reviewed. Different types of solar cells are selected as photoelectric conversion devices to provide power for water electrolysis devices, such as silicon solar cells (SSCs), perovskite solar cells (PSCs), organic solar cells (OSCs), dye-sensitized solar cells (DSSC) and so on.^[43,44]

Silicon Solar Cells. As the first generation of solar cells, silicon-based solar cells have attracted stupendous interest due to their mature craftsmanship, good stability and high photoelectric conversion efficiency. Coupling silicon solar cells with water electrolysis process is considered as an ideal platform for solar-to-hydrogen conversion. For example, Zhang et al. reported a 24-hour novel water splitting system including a silicon-based solar cell, two Ni-Zn batteries, and a water electrolyzer with zinc-nickel-cobalt phosphide electrocatalysts (Figure 3a).^[45] It is worth noting

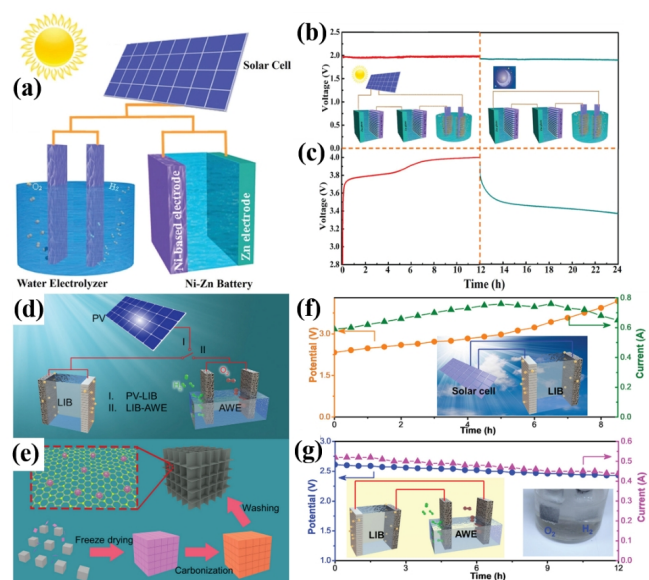


Figure 3. (a) Schematic illustration of the water electrolysis system.^[45] (b) Voltage-time curve of the overall water electrolyzer.^[45] (c) Charging curve and the discharging curve of the Ni-Zn batteries.^[45] (d) Schematic illustration of the PV-LIB and LIB-AWE system.^[46] (e) Schematic illustration of material synthesis process flow.^[46] (f, g) Potential-current-time curve of the PV-LIB and LIB-AWE system, respectively.^[46]

that the silicon-based solar cell enables the convert of solar energy to electricity so as to charge the Ni-Zn batteries during the day. When the batteries are fully charged, the silicon-based solar cell can also directly provide a relatively stable voltage for the water electrolyzer. More importantly, when night falls, the fully charged Ni-Zn batteries can output a stable 1.75 V for the electrolyzer. Figure 3b and 3c demonstrate voltage-time curves of the water electrolyzer and two Ni-Zn batteries with series connection over 24 hours, respectively. The illustration in the set of Figure 3b shows that the solar cell can provide a stable output voltage of 1.97 V within 12 hours, and fully charge two Ni-Zn batteries in series. At night, they can supply power to the water electrolyzer which could work at a relatively stable voltage of 1.93 V for 12 hours. At the same time, the charge-discharge curve of the Ni-Zn batteries is also very stable (Figure 3c). Therefore, it is proved that the integral water decomposition assembly system can store and convert enough solar energy to maintain stable operation. Similarly, Sun et al. constructed a silicon-based solar cell (SSCs)-lithium battery (LIB)-alkaline water electrolysis (AWE) system (Figure 3d) for solar-to-hydrogen application by employing p-NiO@NC as catalyst (Figure 3e).^[46] This system is divided into two parts. One is the solar cell to charge the lithium battery (inset of Figure 3f), and the other is the lithium battery to power the alkaline water electrolysis (inset of Figure 3g). The potential of the lithium battery increases with the charging time and the stable power supply for the alkaline water electrolysis for up to 12 hours illustrates the feasibility of this scheme.

In order to satisfy the practicable overpotential requirements of electrocatalysts, electrolyzers usually need to operate at larger applied photovoltages. Based on this, Pham et al. proposed a unique silicon-based serial cell system,^[47] which includes hydrogen treated amorphous silicon germanium (a-SiGe:H) as the top cell and monocrystalline silicon heterojunction at both ends of the bottom cell (Figure 4a). They leveraged various bandgap engineering techniques to optimize the a-SiGe:H top cell, achieving a

maximum open-circuit voltage (V_{OC}) greater than 1.5 V. Under ideal conditions, when the solar cell is operating at maximum power, it can provide 13.1% STH efficiency. In comparison to the single-junction silicon solar cells, the a-SiGe:H/SHJ based system can produce a sufficiently high voltage while saving the amount of silicon used. In addition, improving the catalytic efficiency of the catalytic electrode and reducing the overpotential of the catalytic reaction are also beneficial for improving the STH efficiency. Lee et al. reported a CoFeVO_x dual-functional electrocatalyst prepared by a simple electrodeposition route.^[48] The most efficient bifunctional $\text{Co}_{0.6}\text{Fe}_{0.3}\text{V}_{0.1}\text{O}_x$ catalyst was incorporated into the electrochemical water splitting system driven by photovoltaic device. The device composed of this module achieved an average STH efficiency of 13.3%. Moreover, it exhibited fairly stable performance during operation and showed an average operating current of -103.92 mA within 2 hours.

Perovskite Solar Cells. Organic-inorganic hybrid perovskite solar cell, as an emerging solar cell, is experiencing rapid development due to their tunable band gap, wide optical absorption range from the visible to near-infrared region (NIR), long-term carrier time and high mobility characteristics, which has attracted great attention of researchers.^[49,50] In recent years, perovskite solar cell-coupled water electrolysis systems have also been gradually explored to pursue efficient solar-to-hydrogen energy conversion.^[51-53]

Considering the effect of electrocatalytic activity of catalyst on the conversion efficiency of electrical energy to hydrogen energy, Parvin et al. designed a semi-crystalline hybrid 2D metal oxide nanosheet (NPL-300) obtained by the conversion of CoFe-LDH at high temperature.^[54] The nanosheet morphology enables NPL-300 with more exposed active sites and enhanced conductivity. Therefore, when it is assembled in an electrolyzer as a bifunctional electrocatalyst, a voltage of 1.69 V is required to provide a current density of 10 mA cm⁻², which is much smaller than that of CoFe-LDH (1.93 V). In the system, a V_{OC} of 2.05 V and a photo-

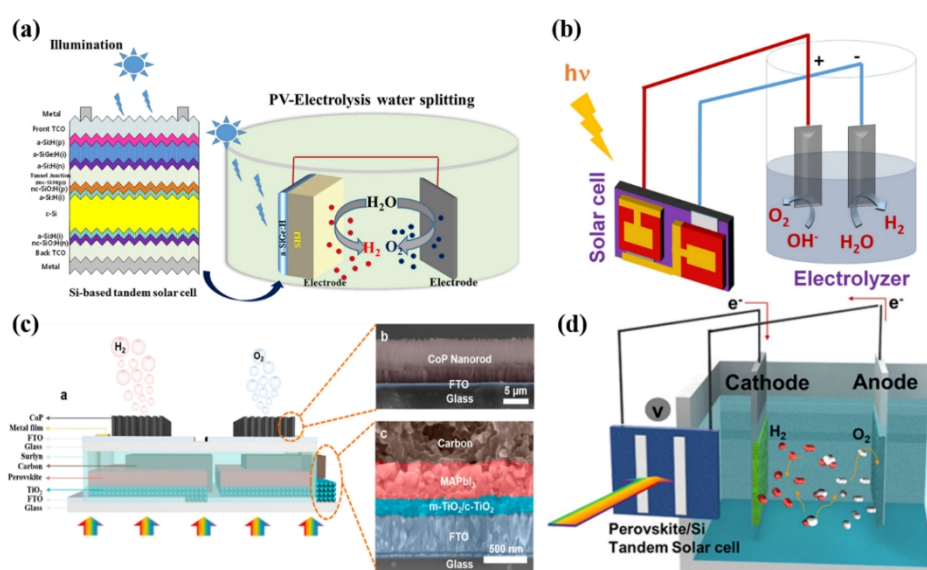


Figure 4. (a) Schematic of electrolysis water system with a-SiGe/SHJ series solar cells as power source.^[47] (b) Schematic illustration of water electrolyzer with PSC.^[54] (c) The structure of the integrated device.^[55] (d) Schematic illustration of the integrated device.^[56]

Table 2. Performance of PV-EC Cells for Water Splitting

PV cell	Electrolyzer cathode anode	STH (%)	Durability (h)	Ref
polycrystalline Si solar cell	ZNCP NWAs/NF ZNCP NWAs/NF	-	24	[45]
crystalline Si solar cell	Co _{0.6} Fe _{0.3} V _{0.1} O _x Co _{0.6} Fe _{0.3} V _{0.1} O _x	13.3	-	[47]
perovskite solar cell	Pt/C Co ₉ S ₈ @MoS ₂	13.6	2	[48]
organic-inorganic halide perovskite solar cell	NPL-300 NPL-300	9.3	-	[54]
perovskite solar cell	CoP CoP	6.7	-	[55]
perovskite/silicon tandem cell	NiMo NiFe LDH	17.52	-	[56]
dye sensitized solar cell	NiMoZn NanoCOT	3.9	5	[58]
dye sensitized solar cell	NiCo ₂ Se ₄ -H NiCo ₂ Se ₄ -H	5.18	-	[59]
dye sensitized solar cell	Fe _{0.37} Ni _{0.17} Co _{0.36} Se Fe _{0.37} Ni _{0.17} Co _{0.36} Se	5.58	-	[60]
commercial silicon-based solar cell	CoFe ₂ O ₄ CoNi LDH/CoFe ₂ O ₄	12.7	-	[61]
commercial GaAs solar cell	Co ₂ P/Mo ₂ C@NC Co ₂ P/Mo ₂ C@NC	18.1	-	[62]
commercial silicon-based solar cell	Ni/Gr/CNTs/Sn ₄ P ₃ Ni/Gr/CNTs/Sn ₄ P ₃	10.82	90	[63]

to-electric conversion efficiency of 12.2% were achieved with two tandem perovskite solar cells (PSCs) (Figure 4b). Moreover, a STH efficiency of 9.3% was observed on this system when connected to the tandem PSCs for unbiased solar-driven overall water splitting. In order to realize the wider application of solar cell-driven water electrolysis system, it is necessary to design efficient integrated devices with low-cost. Liang et al. proposed a wireless compact design to avoid extra ohmic loss, circuit design, and additional device packaging.^[55] The fully integrated hydrogen production system consists of an electrolyzer with two CoP catalyst electrodes and two perovskite solar cells (Figure 4c). The two tandem carbon-based PSCs exhibited photo-to-electric conversion efficiency of 10.6%, while the STH efficiency of the integrated device is as high as 6.7%.

In addition to improving the activity of catalytic electrodes, Park et al. also considered connecting PSCs and silicon solar cells in series to advance the utilization efficiency of solar energy.^[56] The incorporation of Br into the X-site in perovskite solar cells was used to tune the band gap, the current density and photovoltage of the cell. Therefore, they increased the V_{OC} by Br-doped methylammonium lead iodide (MAPb(I_{0.85}Br_{0.15})₃), which is the main component of the light-absorbing layer of PSCs. With this optimized method, the V_{OC} of the solar cell was improved to 1.7 V and the photo-to-electric conversion efficiency reached 23.1%, both exceeding the efficiency of most solar cells. In their system, an electrolyzer with homemade catalytic electrodes was powered by perovskite/Si tandem solar energy (Figure 4d), which achieved the STH efficiency of 17.52%. Therefore, improving the photo-electric conversion efficiency of PSCs is beneficial to construct an efficient solar cell driven water electrolysis hydrogen production system.

Dye Sensitized Solar Cells. In the past decades, dye-sensitized solar cells (known as Gratzel cells) have also been widely studied due to their low cost, simple fabrication process, and abundant raw materials.^[57] Dye sensitized solar cells (DSSCs) are usually composed of photosensitive dyes, redox electrolytes and platinum plated counter electrodes. In recent years, DSSCs and water electrolysis coupled systems have also begun to be explored. To advance the power conversion efficiency of coupled systems, more efforts have been devoted to improving the catalytic activity of electrodes in electrolyzer, which has been discussed in detail

in the previous section. Besides, the modification of dye-sensitized solar cells has attracted some attention.

Cheema et al. constructed an overall water splitting cell with NanoCOT as anodic electrocatalyst and NiMoZn as cathodic electrocatalysts, and the as obtained system was powered by a sequential series multijunction dye-sensitized solar cell (SSM-DSC) without using noble metal.^[58] In this project, the SSM-DSC device was designed to balance transmittance and absorptivity by choosing organic sensitizer without noble metal instead of Ru-based sensitizer, and the photon flux of each subcell was controlled by adjusting the thickness of TiO₂. The driving force for the system came from three series-connected dye-sensitized solar cells with a V_{OC} of 2.4 V. The photo-to-electric efficiency of SSM-DSC device is 8.5%, and a stable STH efficiency of 3.9% is finally obtained.

In addition, Wang et al. firstly prepared a hollow-structured NiCo₂Se₄, which exhibits high catalytic performance in quasi-solid-state DSSCs (QSSDSSCs), HER, and OER.^[59] They assembled QSSDSSCs with NiCo₂Se₄-H as photocathode and TiO₂ as photoanode, and the power conversion efficiency could reach 8.26%. Then, an integrated system is assembled from a triple-junction QSSDSSCs and a water-splitting cell with a STH efficiency of 5.18%. The team subsequently reported a quaternary Fe_{0.37}Ni_{0.17}Co_{0.36}Se that shows good electrocatalytic performance as an electrode in DSSC and for water splitting.^[60] Their prepared QSSDSSCs exhibited a power conversion efficiency of 8.42%. The output voltage of tandem QSSDSSC under a standard sunlight illumination is sufficient to drive water splitting, achieving a STH efficiency of 5.58% in the case of Fe_{0.37}Ni_{0.17}Co_{0.36}Se as electrocatalyst. It can be expected that the use of DSSCs as a power source for water electrolyzers has great prospects. Table 2 shows the solar-to-hydrogen conversion efficiencies of different kinds of solar cells coupled with various catalytic electrode systems.

Thermoelectric Device Hydrogen Production System. The tandem of the water splitting unit with photovoltaic cell is essential in the photovoltaic hydrogen production system, which leads to the device integration conflict between the light absorption of PV cell and the electron diffusion in electrolyte. Fortunately, utilizing the Seebeck effect to achieve energy conversion between solar, thermal, and electrical energy through a thermoelectric generator (TE) provides a promising method to avoid the conflict between

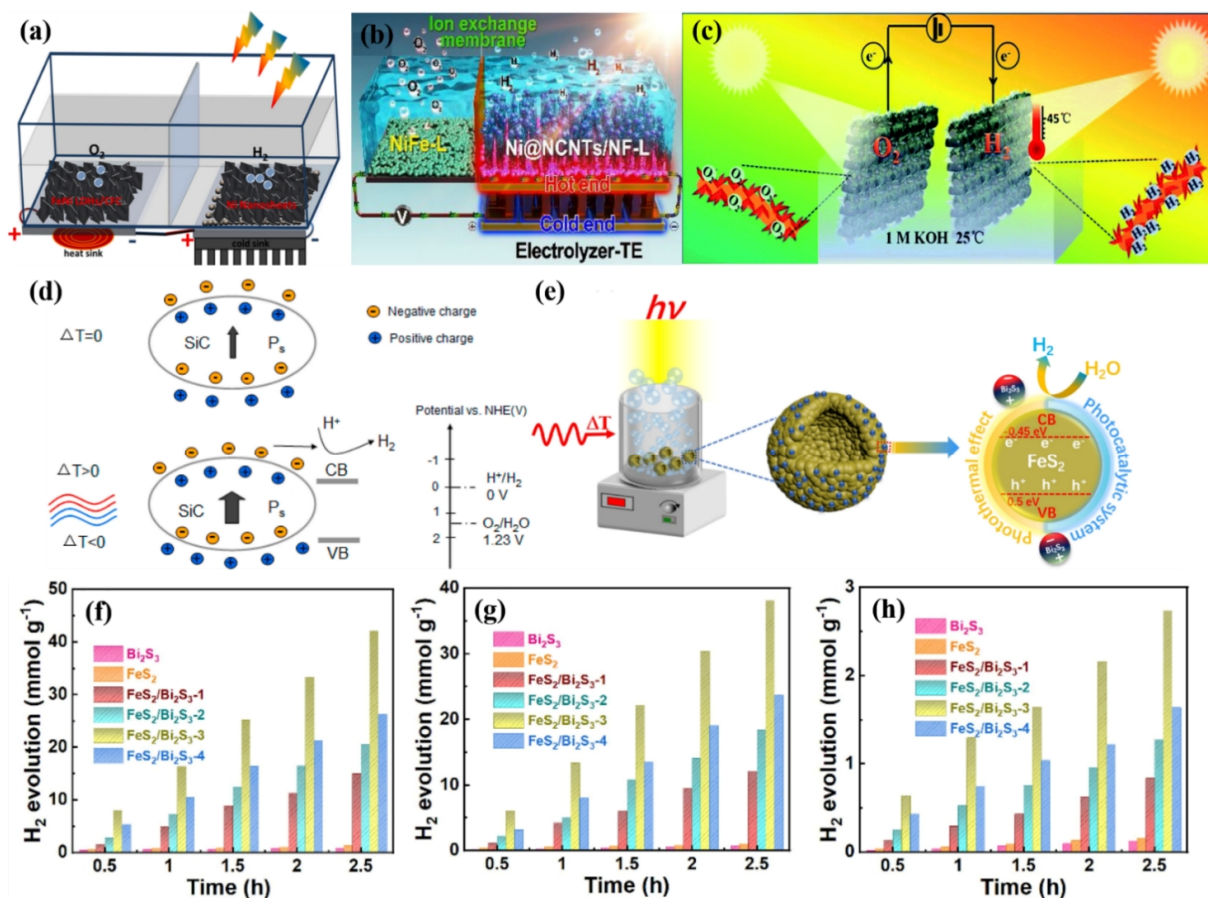


Figure 5. (a) Schematic illustration of Electrolyzer-TE hybrid device.^[66] (b) Schematic illustration of Electrolyzer-TE hybrid device.^[67] (c) Schematic illustration of the photothermal coupling of the Ni-W-B/CC electrode.^[68] (d) Schematic diagram of charge transfer process of SiC.^[71] (e) Schematic illustration of pyroelectric hydrogen production.^[73] Hydrogen evolution curves of different samples under (f) simulated sunlight, (g) and (h) visible light and NIR light.^[73]

PV cell and the water splitting unit, so as to achieve the device integrated.^[64] Combining infrared-active photothermal materials with thermoelectric devices is an effective strategy to convert infrared light into electricity. Specifically, using the surface plasmon resonance (SPR) effect, photothermal materials can convert the absorbed infrared light into thermal energy and transfer it to thermoelectric devices, which can directly convert thermal energy into electrical energy through the Seebeck effect.^[65,66] Therefore, some researchers have carried out extensive researches on such light-thermal-electricity partially or completely replacing the power source to drive the electrolyzer.

The group VIII metals (Au, Ru, Rh, Ni, Co, Pd, Pt, Ir and Fe) based photothermal nanomaterials are frequently studied as light absorption layer for thermoelectric (TE) devices. Therefore, Zhao et al. designed a TE device-assisted water electrolysis system with a multifunctional porous nickel nanosheet array as the cathode electrode and light absorption layer (Figure 5a).^[66] In detail, Ni nanosheet arrays grown on alumina ceramic chips can ensure thermal conductivity and provide temperature difference (ΔT) at the hot side of TE devices (Ni NSs/TE), and according to the Seebeck effect, the difference in temperature of two different conductors causes a potential difference. Due to the three-dimensional

multi-layer structure of porous nanosheet array, the average temperature of Ni nanosheet array/ Al_2O_3 ceramic chip reached 92.2 °C in 2 min under irradiation of the simulated sunlight. When the TE device operated under light irradiation conditions, only an additional external bias voltage of 0.7 V was required to achieve a current density of 10 mA cm⁻². The Electrolyzer-TE coupling device for overall water splitting achieved high hydrogen-evolving rate of 1.818 mmol h⁻¹ and oxygen-evolving rate of 0.912 mmol h⁻¹. Yuan et al. reported a similar system using Ni@NCTs/NF-L as cathode catalyst and photothermal conversion layer (Figure 5b).^[67] In this work, the Ni@NCTs/NF-L cathode and the NiFe alloy foil anode were assembled in an electrolytic cell, which required an applied voltage of 1.947 V to achieve a current density of 50 mA cm⁻². While coupling the electrolytic cell with a TE device, under standard AM 1.5 G illumination, the additional voltage for water splitting was reduced from 1.947 to 1.213 V at a current density of 50 mA cm⁻².

In addition to using the thermoelectric effect to drive the overall water splitting, the photothermal effect (PTE) can be used to locally heat the electrode instead of heating the electrolysis cell, which can effectively improve the water electrolysis performance and save energy. Hao et al. demonstrated that the effect of reduc-

ing the reaction overpotential was achieved by applying external light to the working electrode in order to increase the temperature (Figure 5c).^[68] When the catalyst was operated at 100 mA cm⁻² under light conditioning, the overpotential of HER decreased from 136 to 100 mV, and the overpotential of OER decreased from 367 to 344 mV. When this PTE-coupled electrode was used for full water splitting, only an applied voltage of 1.524 V is required to achieve the 25 mA cm⁻². This work provides a new idea for using convenient photothermal effects to promote electrocatalytic hydrogen production. It can be seen from the above work that combining photothermal materials with thermoelectric materials to drive water electrolysis for hydrogen production can effectively reduce the energy consumption of hydrogen production, which is a good strategy for converting solar energy into clean energy.

Pyroelectric Device Hydrogen Production System. Pyroelectric catalytic hydrogen production is another sustainable hydrogen production technology. The pyroelectric effect refers to the change of the spontaneous polarization state of certain polar materials due to temperature changes. Many electric dipoles in a pyroelectric material are superimposed to form a spontaneous polarization (Ps) state perpendicular to the plane. When the temperature of a pyroelectric material increases ($dT/dt > 0$), the oscillation degree of the electric dipole is enhanced, and the spontaneous polarization is weakened, which further drives the electron migration in the external circuit and reaches a new electrostatic equilibrium state. Likewise, when the temperature drops, the spontaneous polarization is enhanced and the electrical equilibrium is broken again, causing reverse electron migration. O₂ and H⁺ can be generated through the interaction between the resulting positive charge and water. After that, the electrons can reduce H⁺ in aqueous solution to H₂.^[69,70]

As reported by Sun et al., silicon carbide was used as the pyroelectric catalyst in the working electrode.^[71] They put the three-electrode system in an electrolyte with alternating cold and hot for pyroelectric catalytic to produce hydrogen. After that, infrared heating lamps were employed to intermittently heat the working electrode to make the electrolyte temperature circulate in the range of 300–330 K with a cycle of 20 minutes (Figure 5d). Under such cycle test conditions, the hydrogen production per gram of SiC is 32.8 μmol. The results showed that the pyroelectric effect of silicon carbide can be combined with its piezoelectric performance, and it is expected to achieve better catalytic performance. Hexagonal cadmium sulfide (CdS) with an asymmetric central structure also exhibited remarkable pyroelectric properties. Previously, 2-mercaptobenzimidazole (2MBI) modified hexagonal CdS (CdS-2MBI) was reported.^[72] The average hydrogen generation rate is up to 4.3 μmol g⁻¹ per thermal cycle, which is approximately five times that of pure CdS (0.8 μmol g⁻¹). The authors amplified the pyroelectric response of CdS by virtue of the excellent bonding properties and strong hole acceptor ability of 2MBI, which enhanced the charge separation, ultimately leading to higher pyroelectric catalytic hydrogen evolution activity.

However, the change of temperature is easily affected by the external environment and cannot make full use of solar energy. Thus, it is meaningful to use the heat generated by the photothermal effect to provide a more powerful driving force for the pyroe-

lectric effect. In light of this, Li et al. designed a photothermal and pyroelectric effect-assisted photocatalytic hydrogen production system.^[73] The hollow FeS₂ was used as a photothermal layer to provide a heat source for the pyroelectric effect of Bi₂S₃ and also as a photocatalyst. Combining photothermal action with the circulating condensed water environment can continuously generate temperature difference to spontaneously polarize Bi₂S₃ and release surface charges, thereby controlling the movement direction of carriers, inhibiting their recombination, and improving hydrogen production efficiency (Figure 5e). As shown in Figure 5f, the FeS₂/Bi₂S₃-3 photocatalyst showed the highest hydrogen production rate of 16.8 mmol g⁻¹ h⁻¹, which is 32.4 times that of pure FeS₂ (0.52 mmol g⁻¹ h⁻¹). In addition, the photocatalytic hydrogen production rates of different samples under visible and near-infrared light were also investigated (Figure 5 g and h). It is indicated integrating photothermal effect into pyroelectric materials can effectively utilize near-infrared light and improve the utilization efficiency of sunlight. There are also some other pyroelectric hydrogen production systems, Xu et al. reported the direct hydrogen evolution by using the pyroelectric nanomaterial Ba_{0.7}Sr_{0.3}TiO₃ (BST) to harvest energy that came from temperature alternations.^[74] The rate of hydrogen production reached 1.30 μmol g⁻¹ per thermal cycle. These efficient and environmentally friendly pyroelectric devices coupled hydrogen production systems provide great potential for harnessing ambient cold and heat energy.

Piezoelectric Device Hydrogen Production System. The low solar energy utilization and intermittence between day and night are the main reasons that hinder the extensive utilization of PV and PEC water splitting. In the past decade, the collection of vibration energy has attracted a lot of attention. When the piezoelectric device receives the action of vibration energy, it will deform and a piezoelectric field is generated due to the change of the internal polarization state, which can drive the separation of carriers.^[75] The piezoelectric positive charge (q⁺) will react with water molecules to produce H⁺ and O₂. The negative charge (q⁻) reacts with the generated H⁺ to form H₂. For example, Feng et al. reported a piezoelectric catalytic hydrogen production system composed of MoC@NG nanosheets,^[76] which was first used for hydrogen production from pure water by piezo-catalysis. Under the action of mechanical vibration, the ultra-thin N-doped graphene (NG) layer can provide piezoelectric potential to trigger the HER on the MoC quantum dots. The MoC quantum dots, on one hand, can collect free electrons to realize the separation of carrier components, and on the other hand, it can provide abundant and highly active HER sites with low overpotential. In this work, the rate of hydrogen production by piezoelectric catalysis is as high as 169.0 μmol g⁻¹ h⁻¹. The synergy produced by the combination of piezoelectric ultra-thin NG layer and MoC QD is a key factor for efficient hydrogen evolution reaction. Apart from transition carbides, Yu et al. successfully synthesized nano-sized biphasic transition metal nitride Co₄N-WN_x(CWN) through the nitridation of CoWO₄ precursor.^[77] By modulating the non-centrosymmetric structure of CWN, the optimal hydrogen production rate of CWN in pure water is about 262.7 μmol g⁻¹ h⁻¹. The non-centrosymmetric WN_x and its junction with Co₄N contribute to the piezoelectric properties.

As an efficient piezoelectric catalyst, Bi₂WO₆, provides a wide

outlook for hydrogen production by utilizing natural vibrational energy. In the previous work, layered perovskite Bi_2WO_6 nanoplate was employed to catalyze hydrogen production under vibration. Xu et al. solved the problem of recombination of positive and negative charges by adding the sacrificial agent triethanolamine,^[76] which bound to positive charges to further generate H^+ and more stable complexes. At the same time, the effects of temperature and sonochemical effect were excluded when exploring the catalytic performance of piezoelectric materials. The hydrogen production rate of this system reached $191.3 \mu\text{mol g}^{-1} \text{h}^{-1}$ within 6 h, and almost no hydrogen production could be detected when the Bi_2WO_6 nanosheets were removed. In addition, Wang et al. investigated the piezoelectric hydrogen evolution performance of gallium-doped ZnO single crystals without co-catalysts.^[78] Ga-doped ZnO bulk crystals exhibited excellent hydrogen production activity in pure water excited by ultrasound in the dark. The maximum rate of hydrogen generation is $5915 \mu\text{mol h}^{-1} \text{m}^{-2}$ on Ga-doped ZnO crystals. This highly efficient and environmentally friendly piezoelectric catalytic technology provides a wide outlook for hydrogen production from natural vibration energy.

n COMPLEX HYDROGEN PRODUCTION SYSTEMS

To fully utilize solar energy and improve the efficiency of hydrogen production systems, the researchers have been devoted some efforts to the composite system that couples the photoelectrochemical hydrogen production process with the photovoltaic, thermoelectric, pyroelectric and piezoelectric device.

Photovoltaic Device Coupled Photoelectrochemical Hydrogen Production System. The use of photoelectrodes to bring

about STH efficiency close to 20% is still an important step to advance the practical application of PEC hydrogen production technology. The PV-PEC device formed by the series connection of PEC device and photovoltaic solar cell is a promising system, which can bring high STH efficiency at low cost.^[79] Generally speaking, a typical PV-PEC series system consists of a photoelectrode for PEC, a counter electrode and PV components that provide external bias voltage. The photoelectrode absorbs part of the incident light, and the photon energy of this part is equal to or greater than the band gap of the semiconductor photoelectrode. The remaining light that cannot be absorbed by the photoelectrode is absorbed by the subsequent photovoltaic panel. Therefore, the energy in sunlight can be better utilized. Compared with PEC and PV-EC water splitting, the STH efficiency of PV-PEC water splitting has been obviously improved.^[80]

As mentioned earlier, BiVO_4 is a promising photoanode material for PEC water splitting.^[81] However, the limit carrier diffusion length of BiVO_4 offers poor charge separation effect, which hinders its utilization efficiency.^[82] For instance, a $\text{Co}(\text{OH})_2/\text{BiVO}_4$ heterojunction photoanode was produced by a simple solution dipping process.^[83] The results showed that under simulated standard AM 1 sun illumination, the photocurrent density of BiVO_4 was significantly increased from 1.57 to 4.52 mA cm^{-2} at 1.23 V vs RHE with the modification of $\text{Co}(\text{OH})_2$. A PSC- $\text{Co}(\text{OH})_2/\text{BiVO}_4$ series system was also assembled, in which carbon-based PSCs were selected as the photovoltaic device due to its inherent waterproof carbon electrode (Figure 6a).^[84] Such system showed a stable photocurrent density of 3.7 mA cm^{-2} , and achieved a STH efficiency of about 4.6% and an outstanding stability. Similarly, by using a PSC to provide a bias voltage for energy conversion,

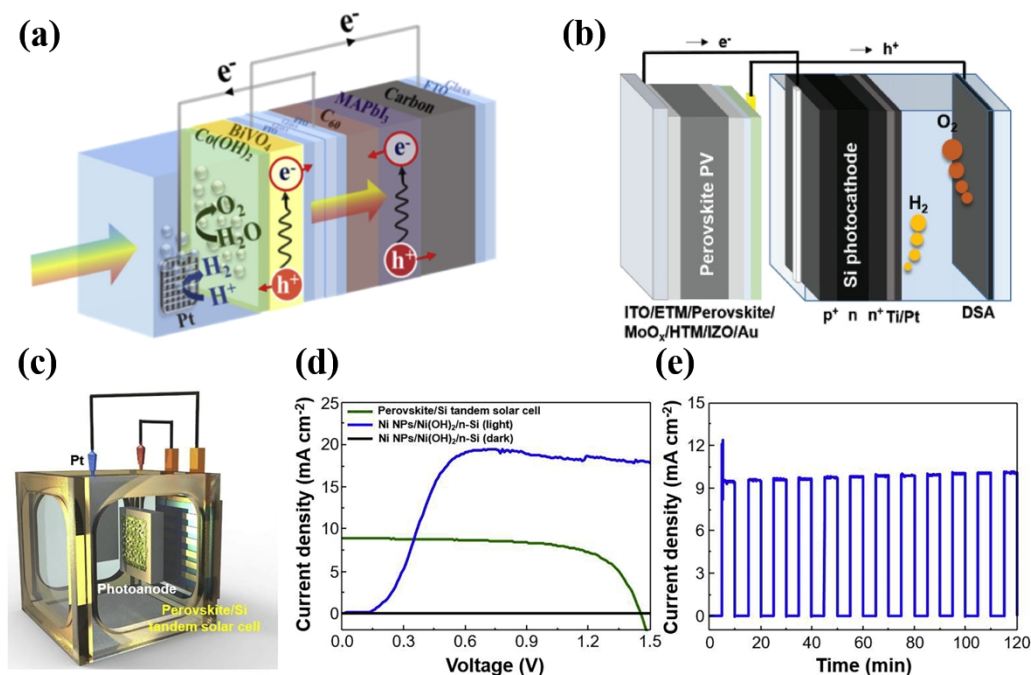


Figure 6. (a) Schematic of PSC- $\text{Co}(\text{OH})_2/\text{BiVO}_4$ tandem system.^[83] (b) Schematic illustration of the tandem system.^[79] (c) Schematic illustration of device composed of Ni NPs/ $\text{Ni}(\text{OH})_2$ /n-Si and perovskite/Si tandem solar cell.^[85] (d) J-V curves of the wired tandem device.^[85] (e) J-T curve of the wired tandem device.^[85]

Karuturi et al. demonstrated an integrated device of silicon photoelectrode and PSC for solar-driven overall water splitting (Figure 6b).^[79] In order to reduce the photovoltage loss caused by poor band energetics, they used a buried p-n junction Si photocathode. Based on this, the p⁺nn⁺-Si/Ti/Pt photocathode was designed and achieved a light stability for more than 3 days and a photocurrent density of 39.7 mA cm⁻² at 0 V vs RHE. When a silicon photocathode was used in series with a high band gap (≈ 1.75 eV) PSC, an unrivalled STH efficiency of more than 17% was obtained. This work proved that the perovskite/silicon double absorber tandem solar cell can independently decompose water. In addition to using PSCs independently, the researchers also developed coupled cells in series with silicon-based solar cells. With the nickel-based catalysts (Ni NPs/Ni(OH)₂), a heterogeneous Ni NPs/Ni(OH)₂/n-Si photoanode was prepared.^[85] Based on this, the authors produced a series device composed of Ni NPs/Ni(OH)₂/n-Si photoanode as internal light absorber and series PSCs as voltage supply (Figure 6c). The power conversion efficiency of the perovskite/Si tandem solar cell is 27.1%. It can be inferred from the JV curve that the integrated device exhibited photocurrent density of 8.8 mA cm⁻² without additional external voltage (Figure 6d). As shown in Figure 6e, without external bias voltage, the photocurrent density generated by the series system in this work is 9.8 mA cm⁻², corresponding to a STH efficiency of 12%.

Thermoelectric Device Coupled Photoelectrochemical Hydrogen Production System. Taking into account the requirements of making full use of solar energy and providing enough energy for spontaneous water splitting, the ideal photoactive material of the photoelectrode in a single photoelectrode PEC cell should have a band gap of about 1.8 eV.^[86] These photoactive materials capture or absorb light with wavelengths less than about 700 nm. In order to expand the utilization range of the solar spectrum, more efforts have been devoted to connecting additional semiconductor light absorbers in series.^[87] For the currently reported PEC water splitting system, most of the infrared region with wavelengths greater than 2500 nm has not been utilized.^[88] To make better use of the energy in this part of the sunlight, the thermoelectric device coupled with a photoelectrode is essential. Kang et al. demonstrated an integrated thermoelectric-assisted PEC system for overall water splitting.^[88] The system uses ΔT between the electrolyte irradiated by incident sunlight as heat source and unirradiated water as cold source to generate bias voltage. In this work, the voltage generated by thermoelectric device is proportional to ΔT . As the temperature difference increased from 10 to 40 °C, the generated voltage increased almost linearly from 102 to 469 mV. The author then tested the overall water splitting performance with a silicon as cathode and a BiVO₄ as anode. Under simulated standard AM 1.5 sun illumination, a 100 mV bias voltage generated by thermoelectric device increased the overall water splitting performance by 1.6 times. The photothermal effect is also utilized to couple with photoelectrochemical catalysis. By introducing the photothermal effect of carbon quantum dots into the PEC water splitting, a coupling system was designed.^[89] When the temperature of CQDs/Fe₂O₃/TiO₂ photoanode rises instantaneously, the charge transfer is stimulated in the photoanode

body due to the photothermal effect. The Co-Pi/CQDs/Fe₂O₃/TiO₂ photoelectrode achieved an obvious photocurrent density of 3 mA cm⁻² at 1.23 V vs RHE. The work confirms that the coupling of the photothermal effect and PEC is feasible and effective.

The above work introduces the Seebeck and photothermal effects into a coupling system for photoelectrochemical catalysis. The additional bias voltage generated by the thermoelectric material and the temperature increase brought about by the photothermal effect both enhance the performance of the photoelectrode for overall water splitting. This strategy offers good direction for the subsequent development of thermoelectrically coupled renewable energy hydrogen production systems.

Pyroelectric Device Coupled Photoelectrochemical Hydrogen Production System. As discussed before, the spontaneous polarization state of pyroelectric materials can easily change with temperature changes, while the charge released can drive water splitting. Therefore, coupling pyroelectric catalysis and photoelectrochemical catalysis that is the combination of illumination and temperature fluctuation can realize "pyroelectric-photoelectrochemical catalysis" in the overall water splitting.^[90]

In addition to possessing photoelectrochemical catalytic ability, barium titanate also exhibits excellent pyroelectric performance owing to the large pyroelectric coefficient (1×10^{-7} C cm⁻² K⁻¹) and appropriate Curie temperature (130 °C).^[91] As such, Zhang et al. proposed pyroelectric-photoelectrochemical catalysis to improve the performance of photoanodes in PEC water splitting by combining pyroelectric catalysis and photoelectrochemical catalysis.^[90] The device exhibited a 0.38 mA cm⁻² current density under alternating cold and heat and light conditions at 1.23 V (vs. RHE), which is significantly higher than the sum of photocurrent density (0.17 mA cm⁻²) and pyroelectric current density (0.13 mA cm⁻²). In another work,^[92] the team combined the pyroelectric effect with the photoelectrochemical properties of NaNbO₃ film to study the impact of pyroelectric effect in the PEC water splitting. Under the heating-cooling cycle of 20-50 °C, NaNbO₃ film exhibited a photocurrent density of 0.37 mA cm⁻² at 1.23 V vs RHE, which is higher than the sum of pyroelectric current density (0.09 mA cm⁻²) and PEC current density (0.14 mA cm⁻²). According to such work, the enhanced photoelectric catalytic efficiency when coupled with pyroelectricity may be due to two aspects: (I) The increase of carrier concentration. (II) The imbalance of polarized charges and the generation of thermoelectric potential result in changes in the energy band structure of the photoelectrode, which accelerates the separation and transfer of charges.^[90]

Piezoelectric Device Coupled Photoelectrochemical Hydrogen Production System. The piezoelectric effect is conducive to the separation and transfer of electric charges.^[93] Therefore, it is promising and meaningful to apply the piezoelectric effect to resolve the high charge recombination rate at the interface during PEC water splitting. Inspired by this fact, Zhang et al. proposed using Pt/ZnO/Co-Pi composite as a photoanode to combine the piezoelectric effect with photoelectrochemistry.^[94] The addition of ultrasonic vibrations causes the ZnO nanorods to bend, generating polarized charges due to the piezoelectric effect (Figure 7a). At the same time, the piezoelectric potential can effectively en-

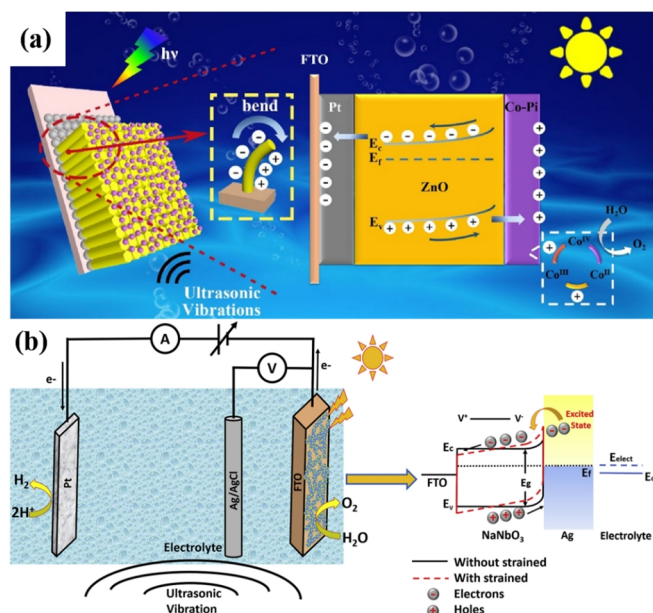


Figure 7. (a) Schematic illustration of the charge generation and transfer mechanism under ultrasonic vibration and light.^[94] (b) Schematic illustration of the system and corresponding energy band diagram of Ag-NaNbO₃/electrolyte interface.^[97]

hance the reaction kinetics. The device exhibited a current density of 0.45 mA cm⁻² at 1.23 V vs RHE. Due to the increase of strain charge and electric field, the current density value is 1.7 times higher than that of ZnO without ultrasonic vibration. Similarly, in order to overcome the high charge recombination rate of ZnO and improve the charge separation efficiency, Chen et al. proposed to couple the ZnO nanorod array with surface WO₃ nanoparticles to construct an efficient direct Z-scheme photoanode.^[95] The optimized ZnO-WO₃-5 showed excellent PEC activities with a photocurrent density of 2.39 mA cm⁻² at 1.23 V vs RHE, which is 2.13 times higher than pure ZnO. And this performance can be further enhanced after introducing stirring as pressure. Z-type heterostructures with significantly improved charge separation efficiency have been widely reported.^[96] Furthermore, Kumar et al. used a simple chemical solution method to synthesize nanocomposite by using silver (Ag) nanoparticles to decorate NaNbO₃ nanorods (Ag-NaNbO₃), and thus realized the coupling of plasma effect and piezo-photoelectric effect.^[97] The experimental results showed that the current density of the Ag-NaNbO₃ photoelectrode is 9 times higher than that of the bare NaNbO₃ under light with ultrasonic vibration. The enhancement of photoelectrochemical catalytic water splitting activity could be attributable to the coupling of piezo-photoelectric and plasmonic effects (Figure 7b). Owing to the existence of silver nanoparticles, the surface plasmon effect optimizes the visible light absorption of nano-NaNbO₃ materials. The piezo-photoelectric effect of nano-NaNbO₃ material is used to generate a built-in electric field to enhance the drift and separation of photo-generated carriers.

n CONCLUSION AND PERSPECTIVE

Converting a steady stream of solar energy directly or indirectly into hydrogen energy is an effective method to cut down the energy consumption of hydrogen production. In this review, recent advances in the coupling design of renewable energy supply devices and catalytic electrodes in various hydrogen production systems are summarized. We not only review the single hydrogen production system based on photochemical, photoelectrochemical, photovoltaic, thermoelectric, pyroelectric and piezoelectric devices, but also discussed the complex systems of multiple devices to realize the sunlight-electricity-hydrogen nexus. We put the emphasis on the structural design and efficiency of applying these energy supply devices to hydrogen production systems.

Excitingly, electrocatalytic materials as well as energy conversion materials such as photoelectrodes, photovoltaic materials, and pyroelectric materials have made great progress in the past few years. Despite many important advances in these energy systems utilizing renewable energy to drive water splitting, the field still faces several challenges. First, the electrocatalytic performance of electrocatalysts in the system is still fundamental. Most of the current non-precious metal electrocatalysts for water splitting only show excellent activity in alkaline condition. With the rapid development of proton exchange membrane (PEM) water electrolyzers, the development of highly active non-precious metal catalysts for HER and OER in PEM is the key to improving the overall efficiency of the system. Therefore, the development of low-cost, highly active, high-stable water splitting electrodes is crucial for industrial applications. Second, the solar energy utilization efficiency of materials such as photovoltaic cells, photoelectrodes, pyroelectric materials, and thermoelectric materials is currently limited. Using a single conversion system is inefficient and may add additional costs due to the series devices with the electrolyzer. Therefore, two or more conversion devices should be combined and integrated into a system to improve the compatibility and integrity of the system for different wavelengths of light. This will reduce the cost of hydrogen energy in actual production in the future. At the same time, some new electrolytic hydrogen production technologies have emerged recently. The direct electrolysis of seawater can not only realize hydrogen production from clean energy, but also use seawater to produce fresh water. Additionally, coastal and inland arid regions are rich in wind energy resources. Unlike conventional wind turbines of the past, the triboelectric nanogenerator (TENG), invented in 2012, is a highly efficient device that converts environmental mechanical energy into electrical energy,^[98] which shows great potential for sustainable and renewable energy applications.

With continuous efforts in the field of hydrogen production from renewable energy sources, water splitting driven by a hybrid clean energy system will make a significant contribution to the large-scale practical application of hydrogen energy. In near future, the renewable energy-based hydrogen production systems will keep an important position in global energy markets, and thus advance the green initiative, sustainable development of human society.

n ACKNOWLEDGEMENTS

This project is financially supported by the Natural Science Foundation of Shanghai (22ZR1471900), Shanghai Municipal Science

and Technology Commission of Carbon Peak&Carbon Neutrality Project (21DZ1207900) and the Hundred Talents Program of the Chinese Academy of Sciences (E13ZB313, E11YB515).

n AUTHOR INFORMATION

Corresponding authors. Emails: wangxianying@mail.sic.ac.cn (X. Wang) and yanya@mail.sic.ac.cn (Y. Yan)

n AUTHOR CONTRIBUTION

These authors contribute equally to the work.

n COMPETING INTERESTS

The authors declare no competing interests.

n ADDITIONAL INFORMATION

Supplementary information is available for this paper at <http://manu30.magtech.com.cn/jghx/EN/10.14102/j.cnki.0254-5861.2022-0106>

For submission: <https://mc03.manuscriptcentral.com/cjsc>

n REFERENCE

- (1) Zhu, Y.; Yue, K.; Xia, C.; Zaman, S.; Yang, H.; Wang, X.; Yan, Y.; Xia, B. Y. Recent advances on MOF derivatives for non-noble metal oxygen electrocatalysts in zinc-air batteries. *Nano Micro. Lett.* **2021**, 13, 137.
- (2) Yue, K.; Liu, J.; Zhu, Y.; Xia, C.; Wang, P.; Zhang, J.; Kong, Y.; Wang, X.; Yan, Y.; Xia, B. Y. In situ ion-exchange preparation and topological transformation of trimetal-organic frameworks for efficient electrocatalytic water oxidation. *Energy Environ. Sci.* **2021**, 14, 6546-6553.
- (3) Yan, Y.; Zhang, J.-Y.; Shi, X.-R.; Zhu, Y.; Xia, C.; Zaman, S.; Hu, X.; Wang, X.; Xia, B. Y. A zeolitic-imidazole framework-derived trifunctional electrocatalyst for hydrazine fuel cells. *ACS Nano* **2021**, 15, 10286-10295.
- (4) IRENA hydrogen from renewable power: technology outlook for the energy transition. <https://www.irena.org/publications/2018/Sep/Hydrogen-from-renewable-power>.
- (5) Zhang, J.-Y.; Yan, Y.; Mei, B.; Qi, R.; He, T.; Wang, Z.; Fang, W.; Zaman, S.; Su, Y.; Ding, S.; Xia, B. Y. Local spin-state tuning of cobalt-iron selenide nanoframes for the boosted oxygen evolution. *Energy Environ. Sci.* **2021**, 14, 365-373.
- (6) Yan, Y.; He, T.; Zhao, B.; Qi, K.; Liu, H.; Xia, B. Y. Metal/covalent-organic frameworks-based electrocatalysts for water splitting. *J. Mater. Chem. A* **2018**, 6, 15905-15926.
- (7) Wu, H.; Tan, H. L.; Toe, C. Y.; Scott, J.; Wang, L.; Amal, R.; Ng, Y. H. Photocatalytic and photoelectrochemical systems: similarities and differences. *Adv. Mater.* **2020**, 32, 1904717.
- (8) Fang, M.; Qin, Q.; Cai, Q.; Liu, W. Transparent Co_3FeO_x film passivated BiVO_4 photoanode for efficient photoelectrochemical water splitting. *Chin. J. Struct. Chem.* **2021**, 40, 1505-1512.
- (9) Hu, C.; Chen, F.; Wang, Y.; Tian, N.; Ma, T.; Zhang, Y.; Huang, H. Exceptional cocatalyst-free photo-enhanced piezocatalytic hydrogen evolution of carbon nitride nanosheets from strong in-plane polarization. *Adv. Mater.* **2021**, 33, 2101751.
- (10) Liu, J.; Gao, Y.; Tang, X.; Zhan, K.; Zhao, B.; Xia, B. Y.; Yan, Y. Metal-organic framework-derived hierarchical ultrathin CoP nanosheets for overall water splitting. *J. Mater. Chem. A* **2020**, 8, 19254-19261.
- (11) Yue, K.; Liu, J.; Xia, C.; Zhan, K.; Wang, P.; Wang, X.; Yan, Y.; Xia, B. Y. Controllable synthesis of multidimensional carboxylic acid-based NiFe

MOFs as efficient electrocatalysts for oxygen evolution. *Mater. Chem. Front.* **2021**, 5, 7191-7198.

(12) Tao, X.; Zhao, Y.; Wang, S.; Li, C.; Li, R. Recent advances and perspectives for solar-driven water splitting using particulate photocatalysts. *Chem. Soc. Rev.* **2022**, 51, 3561-3608.

(13) Zhang, J. Y.; Liao, H. G.; Sun, S. G. Construction of 1D/1D WO_3 nanorod/ TiO_2 nanobelt hybrid heterostructure for photocatalytic application. *Chin. J. Struct. Chem.* **2020**, 39, 1019-1028.

(14) Jiang, X.; Chen, Y. X.; Lu, C. Z. Bio-inspired Materials for photocatalytic hydrogen production. *Chin. J. Struct. Chem.* **2020**, 39, 2123-2130.

(15) Zhan, X.; Fang, Z.; Li, B.; Zhang, H.; Xu, L.; Hou, H.; Yang, W. Rationally designed $\text{Ta}_3\text{N}_5/\text{ReS}_2$ heterojunctions for promoted photocatalytic hydrogen production. *J. Mater. Chem. A* **2021**, 9, 27084-27094.

(16) Ricciarelli, D.; Kaiser, W.; Mosconi, E.; Wiktor, J.; Ashraf, M. W.; Malavasi, L.; Ambrosio, F.; De Angelis, F. Reaction mechanism of photocatalytic hydrogen production at water/tin halide perovskite interfaces. *ACS Energy Lett.* **2022**, 7, 1308-1315.

(17) Li, M. X.; Guan, R. Q.; Li, J. X.; Zhao, Z.; Zhang, J. K.; Dong, C. C.; Qi, Y. F.; Zhai, H. J. Performance and mechanism research of Au-HSTiO_2 on photocatalytic hydrogen production. *Chin. J. Struct. Chem.* **2020**, 39, 1437-1443.

(18) Zhao, H.; Liu, J.; Li, C.-F.; Zhang, X.; Li, Y.; Hu, Z.-Y.; Li, B.; Chen, Z.; Hu, J.; Su, B.-L. Meso-microporous nanosheet-constructed 3DOM perovskites for remarkable photocatalytic hydrogen production. *Adv. Funct. Mater.* **2022**, <https://doi.org/10.1002/adfm.202112831>.

(19) Wu, H.; Tan, H. L.; Toe, C. Y.; Scott, J.; Wang, L.; Amal, R.; Ng, Y. H. Photocatalytic and photoelectrochemical systems: similarities and differences. *Adv. Mater.* **2020**, 32, e1904717.

(20) Do, H. H.; Nguyen, D. L. T.; Nguyen, X. C.; Le, T.-H.; Nguyen, T. P.; Trinh, Q. T.; Ahn, S. H.; Vo, D.-V. N.; Kim, S. Y.; Le, Q. V. Recent progress in TiO_2 -based photocatalysts for hydrogen evolution reaction: a review. *Arabian J. Chem.* **2020**, 13, 3653-3671.

(21) Varunkumar, K.; Sellappan, R. Photoelectrochemical behaviour of $\text{CuBi}_2\text{O}_4/\text{MoS}_2$ photocathode for solar water splitting. *Mater. Chem. Phys.* **2021**, 261, 124245.

(22) Ullah, I.; Munir, A.; Haider, A.; Ullah, N.; Hussain, I. Supported polyoxometalates as emerging nanohybrid materials for photochemical and photoelectrochemical water splitting. *Nanophotonics* **2021**, 10, 1595-1620.

(23) Yang, W.; Kim, J. H.; Hutter, O. S.; Phillips, L. J.; Tan, J.; Park, J.; Lee, H.; Major, J. D.; Lee, J. S.; Moon, J. Benchmark performance of low-cost Sb_2Se_3 photocathodes for unassisted solar overall water splitting. *Nat. Commun.* **2020**, 11, 861.

(24) Li, Y.; Wang, K.; Huang, D.; Li, L.; Tao, J.; Ghany, N. A. A.; Jiang, F. $\text{Cd}_x\text{Zn}_{1-x}\text{S}/\text{Sb}_2\text{Se}_3$ thin film photocathode for efficient solar water splitting. *Appl. Catal., B* **2021**, 286, 119872.

(25) Fujishima, A.; Honda, K. Electrochemical photolysis of water at a semiconductor electrode. *Nature* **1972**, 238, 37-38.

(26) Najaf, Z.; Nguyen, D. L. T.; Chae, S. Y.; Joo, O.-S.; Shah, A. U. H. A.; Vo, D.-V. N.; Nguyen, V.-H.; Le, Q. V.; Rahman, G. Recent trends in development of hematite ($\alpha\text{-Fe}_2\text{O}_3$) as an efficient photoanode for enhancement of photoelectrochemical hydrogen production by solar water splitting. *Int. J. Hydrogen Energy* **2021**, 46, 23334-23357.

(27) Zhu, X.; Liang, X.; Wang, P.; Huang, B.; Zhang, Q.; Qin, X.; Zhang, X. Fabrication of large size nanoporous BiVO_4 photoanode by a printing-

like method for efficient solar water splitting application. *Catal. Today* **2020**, 340, 145-151.

(28) Liu, J.; Chen, W.; Sun, Q.; Zhang, Y.; Li, X.; Wang, J.; Wang, C.; Yu, Y.; Wang, L.; Yu, X. Oxygen vacancies enhanced WO₃/BiVO₄ photoanodes modified by cobalt phosphate for efficient photoelectrochemical water splitting. *ACS Appl. Energy Mater.* **2021**, 4, 2864-2872.

(29) Arifin, K.; Yunus, R. M.; Minggu, L. J.; Kassim, M. B. Improvement of TiO₂ nanotubes for photoelectrochemical water splitting: review. *Int. J. Hydrogen Energy* **2021**, 46, 4998-5024.

(30) Li, C.; Fang, T.; Hu, H.; Wang, Y.; Liu, X.; Zhou, S.; Fu, J.; Wang, W. Synthesis and enhanced bias-free photoelectrochemical water-splitting activity of ferroelectric BaTiO₃/Cu₂O heterostructures under solar light irradiation. *Ceram. Int.* **2021**, 47, 11379-11386.

(31) Zhu, S.-S.; Zhang, Y.; Zou, Y.; Guo, S.-Y.; Liu, H.; Wang, J.-J.; Braun, A. Cu₂S/BiVO₄ Heterostructure photoanode with extended wavelength range for efficient water splitting. *J. Phys. Chem. C* **2021**, 125, 15890-15898.

(32) Zhang, S.; Liu, Z.; Chen, D.; Yan, W. An efficient hole transfer pathway on hematite integrated by ultrathin Al₂O₃ interlayer and novel CuCoO_x cocatalyst for efficient photoelectrochemical water oxidation. *Appl. Catal., B* **2020**, 277, 119197.

(33) Fang, G.; Liu, Z.; Han, C.; Wang, P.; Ma, X.; Lv, H.; Huang, C.; Cheng, Z.; Tong, Z. Promising CoFe-NiOOH ternary polycrystalline cocatalyst for BiVO₄-based photoanodes in photoelectrochemical water splitting. *ACS Appl. Energy Mater.* **2021**, 4, 3842-3850.

(34) Jiao, T.; Lu, C.; Zhang, D.; Feng, K.; Wang, S.; Kang, Z.; Zhong, J. Bi-functional Fe₂ZrO₅ modified hematite photoanode for efficient solar water splitting. *Appl. Catal., B* **2020**, 269, 118768.

(35) Pan, L.; Kim, J. H.; Mayer, M. T.; Son, M.-K.; Ummadisingu, A.; Lee, J. S.; Hagfeldt, A.; Luo, J.; Grätzel, M. Boosting the performance of Cu₂O photocathodes for unassisted solar water splitting devices. *Nat. Catal.* **2018**, 1, 412-420.

(36) Song, A.; Bogdanoff, P.; Esau, A.; Ahmet, I. Y.; Levine, I.; Dittrich, T.; Unold, T.; van de Krol, R.; Berglund, S. P. Assessment of a W:BiVO₄-CuBi₂O₄ tandem photoelectrochemical cell for overall solar water splitting. *ACS Appl. Mater. Interfaces* **2020**, 12, 13959-13970.

(37) Ye, S.; Shi, W.; Liu, Y.; Li, D.; Yin, H.; Chi, H.; Luo, Y.; Ta, N.; Fan, F.; Wang, X.; Li, C. Unassisted photoelectrochemical cell with multimediator modulation for solar water splitting exceeding 4% solar-to-hydrogen efficiency. *J. Am. Chem. Soc.* **2021**, 143, 12499-12508.

(38) Huang, D.; Wang, K.; Li, L.; Feng, K.; An, N.; Ikeda, S.; Kuang, Y.; Ng, Y.; Jiang, F. 3.17% efficient Cu₂ZnSnS₄-BiVO₄ integrated tandem cell for standalone overall solar water splitting. *Energy Environ. Sci.* **2021**, 14, 1480-1489.

(39) Zhou, H.; Feng, M.; Song, K.; Liao, B.; Wang, Y.; Liu, R.; Gong, X.; Zhang, D.; Cao, L.; Chen, S. A highly [001]-textured Sb₂Se₃ photocathode for efficient photoelectrochemical water reduction. *Nanoscale* **2019**, 11, 22871-22879.

(40) Kobayashi, H.; Sato, N.; Orita, M.; Kuang, Y.; Kaneko, H.; Minegishi, T.; Yamada, T.; Domen, K. Development of highly efficient CuIn_{0.5}Ga_{0.5}Se₂-based photocathode and application to overall solar driven water splitting. *Energy Environ. Sci.* **2018**, 11, 3003-3009.

(41) Jang, J.-W.; Du, C.; Ye, Y.; Lin, Y.; Yao, X.; Thorne, J.; Liu, E.; McMahon, G.; Zhu, J.; Javey, A.; Guo, J.; Wang, D. Enabling unassisted solar water splitting by iron oxide and silicon. *Nat. Commun.* **2015**, 6, 7447.

(42) Hayashi, T.; Niishiro, R.; Ishihara, H.; Yamaguchi, M.; Jia, Q.; Kuang,

Y.; Higashi, T.; Iwase, A.; Minegishi, T.; Yamada, T.; Domen, K.; Kudo, A. Powder-based (CuGa_{1-y}In_y)_{1-x}Zn_{2x}S₂ solid solution photocathodes with a largely positive onset potential for solar water splitting. *Sust. Energy Fuels* **2018**, 2, 2016-2024.

(43) Fukuda, K.; Yu, K.; Someya, T. The future of flexible organic solar cells. *Adv. Energy Mater.* **2020**, 10, 2000765.

(44) Ji, J.-M.; Zhou, H.; Eom, Y. K.; Kim, C. H.; Kim, H. K. 14.2% Efficiency dye-sensitized solar cells by Co-sensitizing novel thieno[3,2-b]indole-based organic dyes with a promising porphyrin sensitizer. *Adv. Energy Mater.* **2020**, 10, 2000124.

(45) Zhang, Q.; He, B.; Tang, L.; Zhou, Z.; Kang, L.; Sun, J.; Zhang, T.; Li, Q.; Li, C.; Zhao, J.; Zhang, Z.; Wei, L.; Yao, Y. Fully solar-powered uninterrupted overall water-splitting systems. *Adv. Funct. Mater.* **2019**, 29, 1808889.

(46) Sun, Z.; Wang, G.; Koh, S. W.; Ge, J.; Zhao, H.; Hong, W.; Fei, J.; Zhao, Y.; Gao, P.; Miao, H.; Li, H. Solar-driven alkaline water electrolysis with multifunctional catalysts. *Adv. Funct. Mater.* **2020**, 30, 2002138.

(47) Pham, D. P.; Lee, S.; Le, A. H. T.; Cho, E.-C.; Hyun Cho, Y.; Yi, J. Monocrystalline silicon-based tandem configuration for solar-to-hydrogen conversion. *Inorg. Chem. Commun.* **2020**, 116, 107926.

(48) Lee, M.; Ding, X.; Banerjee, S.; Krause, F.; Smirnov, V.; Astakhov, O.; Merdzhanova, T.; Klingebiel, B.; Kirchartz, T.; Finger, F.; Rau, U.; Haas, S. Bifunctional CoFeVO_x catalyst for solar water splitting by using multijunction and heterojunction silicon solar cells. *Adv. Mater. Technol.* **2020**, 5, 2000592.

(49) Wang, S.; Ma, Z.; Liu, B.; Wu, W.; Zhu, Y.; Ma, R.; Wang, C. High-performance perovskite solar cells with large grain-size obtained by using the lewis acid-base adduct of thiourea. *Sol. RRL* **2018**, 2, 1800034.

(50) Qian, F.; Yuan, S.; Cai, Y.; Han, Y.; Zhao, H.; Sun, J.; Liu, Z.; Liu, S. Novel surface passivation for stable FA_{0.85}MA_{0.15}PbI₃ perovskite solar cells with 21.6% efficiency. *Sol. RRL* **2019**, 3, 1900072.

(51) Yu, Y.; Zhang, F.; Yu, H. Self-healing perovskite solar cells. *Sol. Energy* **2020**, 209, 408-414.

(52) Kim, J. Y.; Lee, J.-W.; Jung, H. S.; Shin, H.; Park, N.-G. High-efficiency perovskite solar cells. *Chem. Rev.* **2020**, 120, 7867-7918.

(53) Tang, G.; You, P.; Tai, Q.; Wu, R.; Yan, F. Performance enhancement of perovskite solar cells induced by lead acetate as an additive. *Sol. RRL* **2018**, 2, 1800066.

(54) Parvin, S.; Chaudhary, D. K.; Ghosh, A.; Bhattacharyya, S. Attuning the electronic properties of two-dimensional Co-Fe-O for accelerating water electrolysis and photolysis. *ACS Appl. Mater. Interfaces* **2019**, 11, 30682-30693.

(55) Liang, J.; Han, X.; Qiu, Y.; Fang, Q.; Zhang, B.; Wang, W.; Zhang, J.; Ajayan, P. M.; Lou, J. A low-cost and high-efficiency integrated device toward solar-driven water splitting. *ACS Nano* **2020**, 14, 5426-5434.

(56) Park, H.; Park, I. J.; Lee, M. G.; Kwon, K. C.; Hong, S.-P.; Kim, D. H.; Lee, S. A.; Lee, T. H.; Kim, C.; Moon, C. W.; Son, D.-Y.; Jung, G. H.; Yang, H. S.; Lee, J. R.; Lee, J.; Park, N.-G.; Kim, S. Y.; Kim, J. Y.; Jang, H. W. Water splitting exceeding 17% solar-to-hydrogen conversion efficiency using solution-processed Ni-based electrocatalysts and perovskite/Si tandem solar cell. *ACS Appl. Mater. Interfaces* **2019**, 11, 33835-33843.

(57) Venkatraman, V.; Raju, R.; Oikonomopoulos, S. P.; Alsberg, B. K. The dye-sensitized solar cell database. *J. Cheminf.* **2018**, 10, 18.

(58) Cheema, H.; Watson, J.; Shinde, P. S.; Rodrigues, R. R.; Pan, S.; Delcamp, J. H. Precious metal-free solar-to-fuel generation: SSM-DSCs powering water splitting with NanoCOT and NiMoZn electrocatalysts.

Chem. Commun. **2020**, 56, 1569-1572.

(59) Wang, M.; Ge, H.; Jin, Z.; Wang, Y.; Zhang, M.; Zheng, G.; Wang, Z.-S. Hollow NiCo₂Se₄ microspheres composed of nanoparticles as multifunctional electrocatalysts for unassisted artificial photosynthesis. *Electrochim. Acta* **2018**, 283, 628-637.

(60) Wang, M.; Li, Y.; Feng, C.; Zhao, G.; Wang, Z.-S. Quaternary iron nickel cobalt selenide as an efficient electrocatalyst for both quasi-solid-state dye-sensitized solar cells and water splitting. *Chem.-Asian J.* **2019**, 14, 1034-1041.

(61) Si, F.; Wei, M.; Li, M.; Xie, X.; Gao, Q.; Cai, X.; Zhang, S.; Peng, F.; Fang, Y.; Yang, S. Natural light driven photovoltaic-electrolysis water splitting with 12.7% solar-to-hydrogen conversion efficiency using a two-electrode system grown with metal foam. *J. Power Sources* **2022**, 538, 231536.

(62) Sun, P.; Zhou, Y.; Li, H.; Zhang, H.; Feng, L.; Cao, Q.; Liu, S.; W'gberg, T.; Hu, G. Round -the-clock bifunctional honeycomb-like nitrogen-doped carbon-decorated Co₂P/Mo₂C-heterojunction electrocatalyst for direct water splitting with 18.1% STH efficiency. *Appl. Catal., B* **2022**, 310, 121354.

(63) Riyajuddin, S.; Pahuja, M.; Sachdeva, P. K.; Azmi, K.; Kumar, S.; Afshan, M.; Ali, F.; Sultana, J.; Maruyama, T.; Bera, C.; Ghosh, K. Super-hydrophilic leaflike Sn₄P₃ on the porous seamless graphene-carbon nanotube heterostructure as an efficient electrocatalyst for solar-driven overall water splitting. *ACS Nano* **2022**, 16, 4861-4875.

(64) Kwan, T. H.; Wu, X. Power and mass optimization of the hybrid solar panel and thermoelectric generators. *Appl. Energy* **2016**, 165, 297-307.

(65) Telkes, M. Solar thermoelectric generators. *J. Appl. Phys.* **1954**, 25, 765-777.

(66) Zhao, L.; Yang, Z.; Cao, Q.; Yang, L.; Zhang, X.; Jia, J.; Sang, Y.; Wu, H.-J.; Zhou, W.; Liu, H. An earth-abundant and multifunctional Ni nanosheets array as electrocatalysts and heat absorption layer integrated thermoelectric device for overall water splitting. *Nano Energy* **2019**, 56, 563-570.

(67) Yuan, H.; Liu, F.; Xue, G.; Liu, H.; Wang, Y.; Zhao, Y.; Liu, X.; Zhang, X.; Zhao, L.; Liu, Z.; Liu, H.; Zhou, W. Laser patterned and bifunctional Ni@N-doped carbon nanotubes as electrocatalyst and photothermal conversion layer for water splitting driven by thermoelectric device. *Appl. Catal., B* **2021**, 283, 119647.

(68) Hao, W.; Wu, R.; Yang, H.; Guo, Y. Photothermal coupling electrolysis on Ni-W-B toward practical overall water splitting. *J. Mater. Chem. A* **2019**, 7, 12440-12445.

(69) Wang, C.; Tian, N.; Ma, T.; Zhang, Y.; Huang, H. Pyroelectric catalysis. *Nano Energy* **2020**, 78, 105371.

(70) Zhang, D.; Wu, H.; Bowen, C. R.; Yang, Y. Recent advances in pyroelectric materials and applications. *Small* **2021**, 17, 2103960.

(71) Sun, S.; Song, L.; Zhang, S.; Sun, H.; Wei, J. Pyroelectric hydrogen production performance of silicon carbide. *Ceram. Int.* **2021**, 47, 20486-20493.

(72) Zhang, M.; Hu, Q.; Ma, K.; Ding, Y.; Li, C. Pyroelectric effect in CdS nanorods decorated with a molecular Co-catalyst for hydrogen evolution. *Nano Energy* **2020**, 73, 104810.

(73) Li, M.; Sun, J.; Chen, G.; Yao, S.; Cong, B.; Liu, P. Construction photothermal/pyroelectric property of hollow FeS₂/Bi₂S₃ nanostructure with enhanced full spectrum photocatalytic activity. *Appl. Catal., B* **2021**, 298, 120573.

(74) Xu, X.; Xiao, L.; Jia, Y.; Wu, Z.; Wang, F.; Wang, Y.; Haugen, N. O.;

Huang, H. Pyro-catalytic hydrogen evolution by Ba_{0.7}Sr_{0.3}TiO₃ nanoparticles: harvesting cold-hot alternation energy near room-temperature. *Energy Environ. Sci.* **2018**, 11, 2198-2207.

(75) Hinchet, R.; Khan, U.; Falconi, C.; Kim, S.-W. Piezoelectric properties in two-dimensional materials: simulations and experiments. *Mater. Today* **2018**, 21, 611-630.

(76) Feng, W.; Yuan, J.; Gao, F.; Weng, B.; Hu, W.; Lei, Y.; Huang, X.; Yang, L.; Shen, J.; Xu, D.; Zhang, X.; Liu, P.; Zhang, S. Piezopotential-driven simulated electrocatalytic nanosystem of ultrasmall MoC quantum dots encapsulated in ultrathin N-doped graphene vesicles for superhigh H₂ production from pure water. *Nano Energy* **2020**, 75, 104990.

(77) Yu, J.; Guo, H.; Feng, W.; Guo, X.; Zhu, Y.; Thomas, T.; Jiang, C.; Liu, S.; Yang, M. Co₄N-WN_x composite for high-efficiency piezocatalytic hydrogen evolution. *Dalton Trans.* **2022**, 51, 7127-7134.

(78) Wang, B.; Zhang, Q.; He, J.; Huang, F.; Li, C.; Wang, M. Co-catalyst-free large ZnO single crystal for high-efficiency piezocatalytic hydrogen evolution from pure water. *J. Energy Chem.* **2022**, 65, 304-311.

(79) Karuturi, S. K.; Shen, H.; Sharma, A.; Beck, F. J.; Varadhan, P.; Duong, T.; Narangari, P. R.; Zhang, D.; Wan, Y.; He, J.-H.; Tan, H. H.; Jagadish, C.; Catchpole, K. Over 17% Efficiency stand-alone solar water splitting enabled by perovskite-silicon tandem absorbers. *Adv. Energy Mater.* **2020**, 10, 2000772.

(80) Chen, Y.; Feng, X.; Liu, Y.; Guan, X.; Burda, C.; Guo, L. Metal oxide-based tandem cells for self-biased photoelectrochemical water splitting. *ACS Energy Lett.* **2020**, 5, 844-866.

(81) Zhang, B.; Wang, L.; Zhang, Y.; Ding, Y.; Bi, Y. Ultrathin FeOOH nanolayers with abundant oxygen vacancies on BiVO₄ photoanodes for efficient water oxidation. *Angew. Chem. Int. Ed.* **2018**, 57, 2248-2252.

(82) Jiang, C.; Moniz, S. J. A.; Wang, A.; Zhang, T.; Tang, J. Photoelectrochemical devices for solar water splitting-materials and challenges. *Chem. Soc. Rev.* **2017**, 46, 4645-4660.

(83) Li, X.; Jia, M.; Lu, Y.; Li, N.; Zheng, Y.-Z.; Tao, X.; Huang, M. Co(OH)₂/BiVO₄ photoanode in tandem with a carbon-based perovskite solar cell for solar-driven overall water splitting. *Electrochim. Acta* **2020**, 330, 135183.

(84) Zhou, J.; Hou, J.; Tao, X.; Meng, X.; Yang, S. Solution-processed electron transport layer of N-doped fullerene for efficient and stable all carbon based perovskite solar cells. *J. Mater. Chem. A* **2019**, 7, 7710-7716.

(85) Lee, S. A.; Park, I. J.; Yang, J. W.; Park, J.; Lee, T. H.; Kim, C.; Moon, J.; Kim, J. Y.; Jang, H. W. Electrodeposited heterogeneous nickel-based catalysts on silicon for efficient sunlight-assisted water splitting. *Cell Rep. Phys. Sci.* **2020**, 1, 100219.

(86) Bolton, J. R.; Strickler, S. J.; Connolly, J. S. Limiting and realizable efficiencies of solar photolysis of water. *Nature* **1985**, 316, 495-500.

(87) Zhang, K.; Ma, M.; Li, P.; Wang, D. H.; Park, J. H. Water splitting progress in tandem devices: moving photolysis beyond electrolysis. *Adv. Energy Mater.* **2016**, 6, 1600602.

(88) Kang, Y.; Chen, R.; Zhen, C.; Wang, L.; Liu, G.; Cheng, H.-M. An integrated thermoelectric-assisted photoelectrochemical system to boost water splitting. *Sci. Bull.* **2020**, 65, 1163-1169.

(89) Hu, X.; Huang, J.; Zhao, F.; Yi, P.; He, B.; Wang, Y.; Chen, T.; Chen, Y.; Li, Z.; Liu, X. Photothermal effect of carbon quantum dots enhanced photoelectrochemical water splitting of hematite photoanodes. *J. Mater. Chem. A* **2020**, 8, 14915-14920.

(90) Zhang, S.; Chen, D.; Liu, Z.; Ruan, M.; Guo, Z. Novel strategy for efficient water splitting through pyro-electric and pyro-photo-electric

catalysis of BaTiO₃ by using thermal resource and solar energy. *Appl. Catal., B* **2021**, 284, 119686.

(91) Zhang, J.; Wang, C.; Bowen, C. Piezoelectric effects and electromechanical theories at the nanoscale. *Nanoscale* **2014**, 6, 13314-13327.

(92) Zhang, S.; Zhang, B.; Chen, D.; Guo, Z.; Ruan, M.; Liu, Z. Promising pyro-photo-electric catalysis in NaNbO₃ via integrating solar and cold-hot alternation energy in pyroelectric-assisted photoelectrochemical system. *Nano Energy* **2021**, 79, 105485.

(93) Shi, J.; Starr, M. B.; Xiang, H.; Hara, Y.; Anderson, M. A.; Seo, J.-H.; Ma, Z.; Wang, X. Interface engineering by piezoelectric potential in ZnO-based photoelectrochemical anode. *Nano Lett.* **2011**, 11, 5587-5593.

(94) Zhang, S.; Liu, Z.; Ruan, M.; Guo, Z.; E, L.; Zhao, W.; Zhao, D.; Wu, X.; Chen, D. Enhanced piezoelectric-effect-assisted photoelectrochemical performance in ZnO modified with dual cocatalysts. *Appl. Catal., B* **2020**, 262, 118279.

(95) Chen, Y.; Wang, L.; Gao, R.; Zhang, Y.-C.; Pan, L.; Huang, C.; Liu, K.; Chang, X.-Y.; Zhang, X.; Zou, J.-J. Polarization-enhanced direct Z-scheme ZnO-WO₃-x nanorod arrays for efficient piezoelectric-photoelectrochemical water splitting. *Appl. Catal., B* **2019**, 259, 118079.

(96) Zhou, P.; Yu, J.; Jaroniec, M. All-solid-state z-scheme photocatalytic systems. *Adv. Mater.* **2014**, 26, 4920-4935.

(97) Kumar, D.; Sharma, S.; Khare, N. Piezo-phototronic and plasmonic effect coupled Ag-NaNbO₃ nanocomposite for enhanced photocatalytic and photoelectrochemical water splitting activity. *Renew. Energy* **2021**, 163, 1569-1579.

(98) Fan, F.-R.; Tian, Z.-Q.; Wang, Z. L. Flexible triboelectric generator. *Nano Energy* **2012**, 1, 328-334.

Received: May 3, 2022

Accepted: May 18, 2022

Published: May 20, 2022



Wei-quan Ji received his bachelor's degree of engineering from Zhejiang University of Water Resources and Electric Power in 2020. Then, he was admitted to University of Shanghai for Science and Technology to pursue his M.S under the guidance of Dr. Ke Zhan. At the same time, he was jointly cultivated at the Shanghai Institute of Ceramics, Chinese Academy of Sciences under the guidance of Dr. Ya Yan. His research interest is focused on the application of nano-functional materials in electrocatalysis.



Kang Zhang received his bachelor of Science degree from Shanxi Datong University in 2020. Then, he was admitted to University of Shanghai for Science and Technology to pursue his M.S under the guidance of Dr. Ke Zhan. At the same time, he was jointly cultivated at the Shanghai Institute of Ceramics, Chinese Academy of Sciences under the guidance of Dr. Ya Yan. His research interest is focused on the application of nano-functional materials in electrocatalytic water splitting.



Prof. Xianying Wang is currently a researcher at the Shanghai Institute of Ceramics, Chinese Academy of Sciences (SICCAS). She received her Ph.D. under the supervision of Academician Gan Fuxi from Shanghai Institute of Optics and Fine Mechanics, Chinese Academy of Sciences (SIOFMCAS) in 2005. In recent years, the research direction mainly focuses on the application of nano-functional materials in the fields of photo/electrocatalysis and energy conversion.



Dr. Ya Yan is currently an Associate Professor of Shanghai Institute of Ceramics, Chinese Academy of Sciences (SICCAS). She received her bachelor's degree in Chemical Engineering from Northwest University (China) in 2010 and earned her Ph.D. degree under the supervision of Professor Xin Wang at Nanyang Technological University (NTU) in 2015. Her recent research interests are in the areas of nanostructured functional materials and their application in energy and environments.